# Distortion in Angle-Modulated Links Induced by Ripple in Fiber-Bragg-Grating Reflectance and Delay Characteristics

Todd G. Ulmer, *Member, IEEE, Member, OSA*

***Abstract*—Ripple in the reflectance and delay characteristics of a linearly chirped fiber Bragg grating is shown to produce significant distortion in a wide-band angle-modulated fiber-optic link. Experimental results for a 7-GHz 39.4-km link where dispersion is compensated with a linearly chirped fiber Bragg grating show that the residual ripple in both the reflectance and delay contributes to harmonic and intermodulation distortion. Numerical modeling shows that the distortion is dominated by the random component of the delay ripple. The distortion is further quantified as a function of the ripple, the modulation index, and the modulation frequency.**

***Index Terms*—Frequency modulation, optical fiber communication, optical fiber devices, phase modulation.**

## I. Introduction

CHIRPED fiber Bragg gratings (CFBGs) have been widely investigated because of their flexible dispersion characteristics, low insertion loss, compact size, and potential for tunability [1]–[10]. The most commonly considered application is dispersion compensation in digital links; however, CFBGs may prove even more useful in wide-band analog fiber-optic links, where dispersion compensation is essential to avoid destructive interference from dispersed sidebands [11]–[13]. In addition to dispersion compensation, advanced optical signal-processing applications such as reconfigurable pulse shaping [14] and polarization-mode-dispersion compensation [15] have been demonstrated using CFBGs. FM discriminators based on chirped Bragg gratings in either fiber [16] or integrated-optic form [17] have also been proposed.

In practical CFBGs, nonideal characteristics such as reflectance and delay ripple can impose performance limitations. Delay ripple in CFBGs has two components: an intrinsic component that can be minimized through proper apodization and a residual component caused by fabrication imperfections [18]. CFBG delay ripple causes phase shifts between the different frequency components of a modulated optical signal and has been shown to produce a small but measurable penalty in both digital systems [19]–[25] and intensity-modulated analog systems [26]–[28]. The effects are most pronounced when the ripple period is comparable to the modulation frequency [29], [30].

Manuscript received April 25, 2003; revised September 9, 2003. This work was supported by the Department of the Air Force under Contract F19628-00-C-0002.

The author is with Lincoln Laboratory, Massachusetts Institute of Technology, Lexington, MA 02420 USA (e-mail: ulmer@ll.mit.edu).

Digital Object Identifier 10.1109/JLT.2003.821717

A more significant limitation can occur in wide-band angle-modulated systems, where several sidebands are generated and their relative amplitude and phase relationship must be preserved to maintain the integrity of the signal. Distortion via conversion from angle modulation to intensity modulation [31], [32] can result from the relative phase shifts between the different sidebands induced by the CFBG. Likewise, ripple in the reflectance of a CFBG produces amplitude variations between the different sidebands, which can also result in distortion. Thus, distortion from both reflectance and delay ripple can potentially be a significant limitation in wide-band angle-modulated systems.

Here, the effects of CFBG reflectance and delay ripple are investigated in a 7-GHz 39.4-km angle-modulated link. Dispersion compensation is accomplished alternately with a CFBG and an equivalent length of dispersion compensating fiber to isolate the ripple-induced effects. Both harmonic and intermodulation distortion are characterized. Numerical modeling of the link using measured characteristics of the CFBG reveals that the distortion is dominated by the random component of the delay ripple. Furthermore, the distortion is quantified as a function of the ripple, the modulation index, and the modulation frequency.

## II. Theory

A carrier with angular frequency $\omega_c$ that is frequency-modulated by a sinusoidal signal with angular frequency $\Omega_m$ can be represented by the sum of its individual frequency components [33]

$$e_{\mathrm{FM}}(t) = \mathrm{Re}\left[E_{\mathrm{o}} \sum_{n=-\infty}^{\infty} J_n(\beta) \exp\left(j\left(\omega_c + n\Omega_m\right)t\right)\right] \quad (1)$$

where the modulation index $\beta$ is given by the ratio of the maximum frequency deviation to the modulation frequency. Upon transmission through the fiber channel, the amplitude of each frequency component is multiplied by a complex transmission coefficient, given by $C_n = A(\omega_n)\exp(j\phi(\omega_n))$, which represents the amplitude and phase response of the channel at that particular frequency. The complex coefficients can be determined from the measured transmission spectrum $\mathrm{T}(\omega)$ and group delay $\tau(\omega)$ of the channel via

$$A(\omega) = \sqrt{T(\omega)} \quad (2)$$

and

$$\phi(\omega) = -\int \tau(\omega) d\omega. \quad (3)$$

0733-8724/03$17.00 © 2003 IEEE

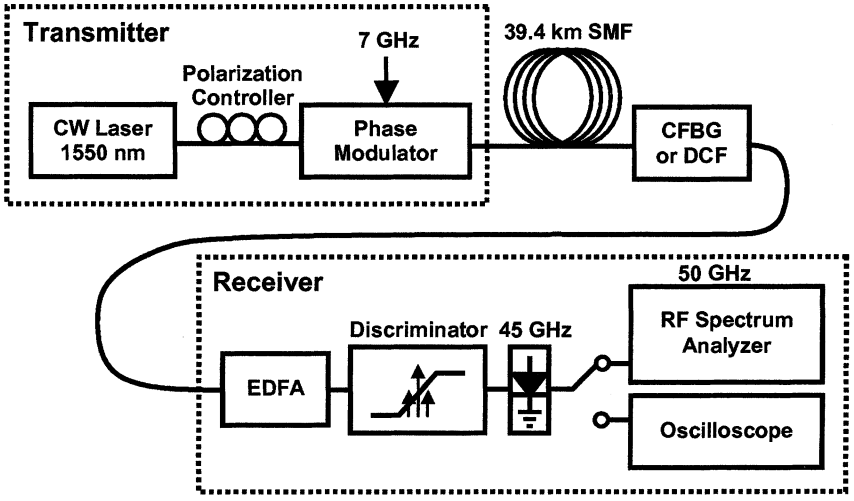


Fig. 1. Experimental setup of the angle-modulated link.

For distortionless transmission, the relative amplitudes of the different frequency components must be preserved, and all components must arrive at the receiver with the same propagation delay. In the presence of frequency-dependent loss and delay, such as that induced by the reflectance and delay ripple of a CFBG, distortion occurs.

Over a small bandwidth, where the amplitude and period of the ripple is approximately constant, the reflectance and group delay of a linearly chirped FBG can be modeled as [19], [30]

$$R \approx R_{\rm o} + A_R \sin\left(\frac{\omega}{T_R} + \theta_R\right) \tag{4}$$

and

$$\tau \approx \tau_{\rm o} + \tau_1 \omega + A_{\rm GDR} \sin\left(\frac{\omega}{T_{\rm GDR}} + \theta_{\rm GDR}\right) \tag{5}$$

where $A_R$, $A_{\rm GDR}$, $T_R$, and $T_{\rm GDR}$ are the amplitudes and periods of the reflectance and group-delay ripples. Using (3), the phase distortion resulting from the group-delay ripple is of the form

$$\phi_{\rm GDR} = A_{\rm GDR} T_{\rm GDR} \cos\left(\frac{\omega}{T_{\rm GDR}} + \theta_{\rm GDR}\right) \tag{6}$$

and thus the amplitude of the phase distortion increases with both the amplitude and the period of the ripple.

As will be observed below, the ripple characteristics of a practical grating can differ significantly from that of a simple sinusoidal model. Thus, the measured characteristics of the grating are critical for accurate modeling of the performance.

## III. Experiments

### A. Angle-Modulated Link

The ripple-induced effects of a CFBG designed for dispersion compensation were examined via comparison with an equivalent length of dispersion compensating fiber (DCF). Experiments were performed using the angle-modulated link shown in Fig. 1. The transmitter consists of a continuous-wave external-cavity laser modulated by an electrooptic phase modulator to produce an angle-modulated signal. The link itself consists of 39.4 km of standard non-dispersion-shifted fiber followed by either the commercial CFBG dispersion compensation module or an equivalent length of DCF. The group-delay slope for the standard fiber, the CFBG, and the DCF were found to be $+653$, $-654$, and $-654$ ps/nm, respectively, using the modulation phase-shift technique [34], [35]. The transmission and group delay of both the standard fiber and the DCF vary smoothly with wavelength; in contrast, the CFBG module exhibits ripple in both its transmission and group-delay characteristics, as described below.

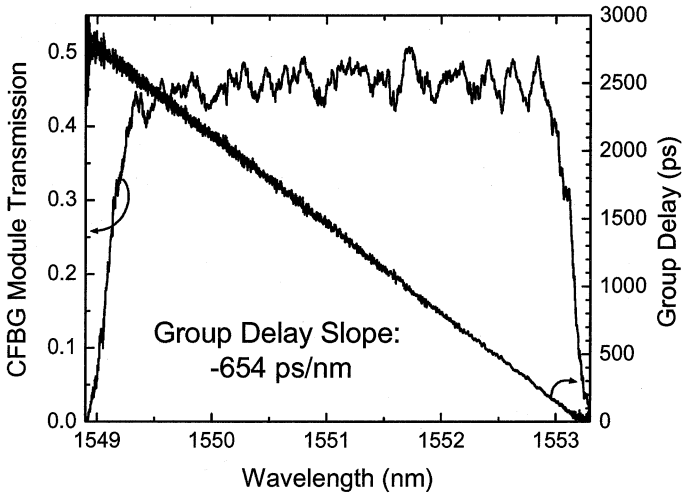


Fig. 2. Measured transmission and group delay of the CFBG dispersion compensation module.

The receiver consists of an erbium-doped fiber amplifier (EDFA) followed by a bandpass filter tuned slightly away from the center wavelength to serve as a discriminator. The recovered intensity-modulated signal is monitored with a 45-GHz photodetector and 50-GHz sampling oscilloscope. Experiments were also performed with the EDFA following the discriminator rather than preceding it with no discernable change in

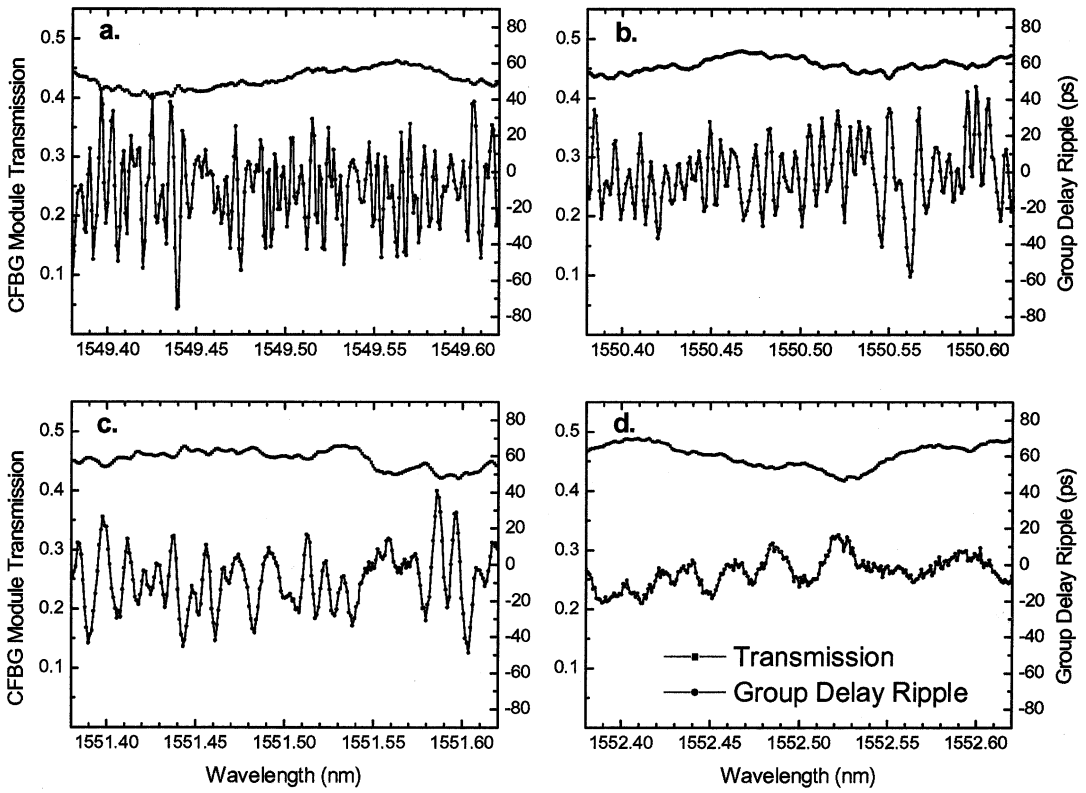


Fig. 3. CFBG module transmission and group-delay ripple near (a) 1549.5 nm, (b) 1550.5 nm, (c) 1551.5 nm, and (d) 1552.5 nm. Note the increase in the period of the group-delay ripple with wavelength.

the results, indicating that the EDFA did not contribute to the observed distortion.

### *B. CFBG Characterization*

Fig. 2 shows the measured transmission and group delay of the CFBG dispersion compensation module, which contains a CFBG packaged with a circulator. The transmission spectrum was measured using an ASE source and an optical spectrum analyzer, and reveals a 4-nm passband centered at 1551.0 nm. The insertion loss is 3.5 $\pm$0.3 dB, with a ripple period on the order of 200 pm (25 GHz). The group delay was determined via the modulation phase-shift technique [34], [35] using a modulation frequency of 50 MHz to ensure accurate results [36], [37]. Indeed, the measured period of the group-delay ripple is on the order of 5 pm (625 MHz) at 1550 nm, necessitating the use of a low modulation frequency to produce an accurate measurement. As shown in Fig. 3, the amplitude of the group-delay ripple ranges from $\pm$50 ps at 1549.5 nm to $\pm$15 ps at 1552.5 nm, whereas the period ranges from $\sim$4 pm at 1549.5 nm to $\sim$20 pm at 1552.5 nm, which is consistent with light entering the CFBG on its long-wavelength side [18]. The group-delay characteristics of the CFBG module have also been verified using commercial instruments based on Jones- and Mueller-matrix analysis [38], confirming the ripple data and the average group-delay slope of $-$654 ps/nm. While the group-delay ripple was found to be very repeatable, the absolute wavelength of the measured pattern was found to vary by up to 20 pm between the different data sets; furthermore, a variation of over 10 pm was observed as the input polarization was changed in consecutive measurements with the same instrument. Thus, the wavelength variation is attributed to a combination of slight calibration errors between the different measurement systems and residual birefringence in the grating.

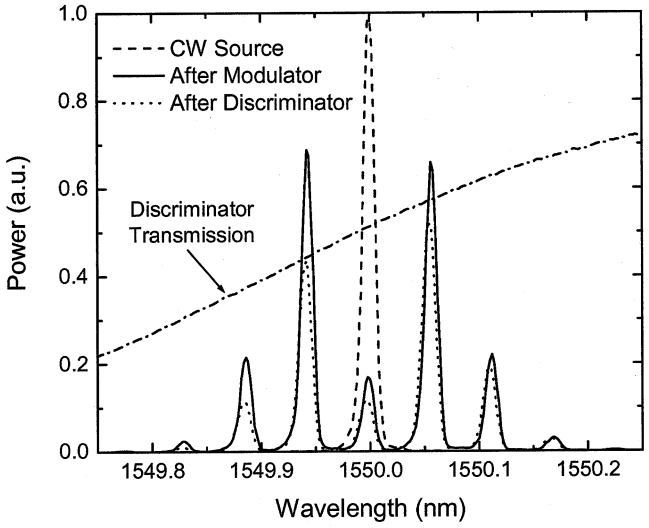


Fig. 4. Optical spectrum of the 7-GHz angle-modulated signal before and after the discriminator.

### *C. Harmonic Distortion Results*

The experimental setup shown in Fig. 1 was used to characterize harmonic distortion at various locations in the link. With a laser wavelength of 1550.000 nm, the phase modulator was

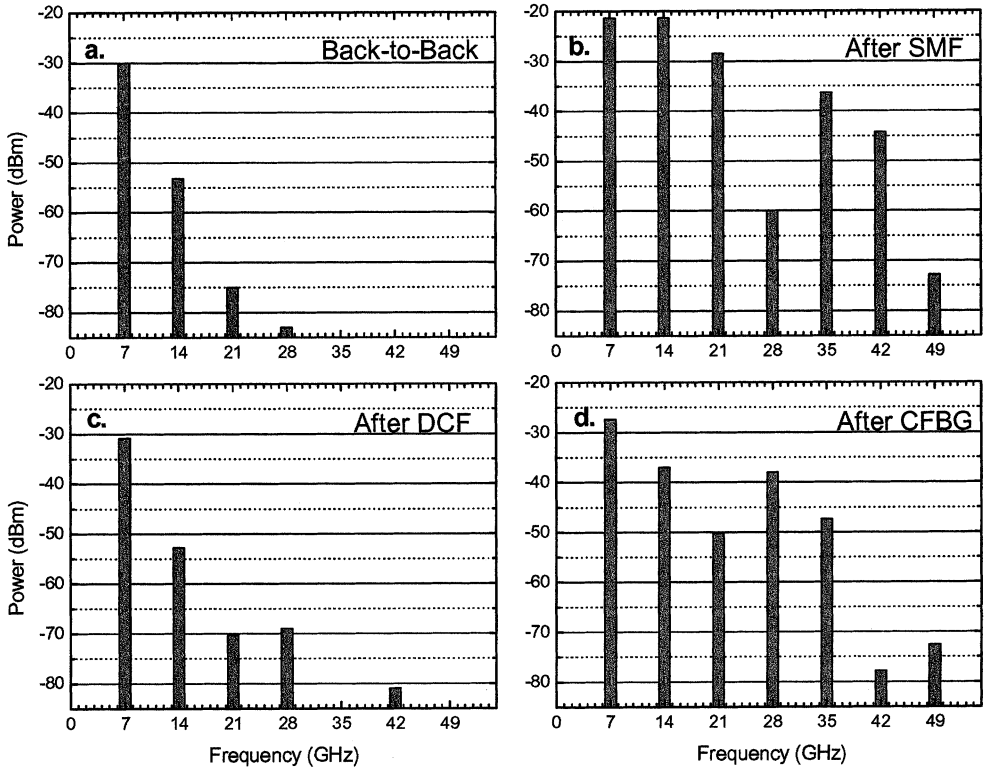


Fig. 5. Harmonic distortion at various points in the angle-modulated link: (a) back-to-back, (b) after 39.4 km of standard fiber, (c) the standard fiber compensated with DCF, and (d) the standard fiber compensated with the CFBG.

driven by a 7.0-GHz sine wave from an RF synthesizer, producing an angle-modulated signal with an FM modulation index of $\beta = 1.9$. Fig. 4 shows the optical power spectra of the transmitter output and the transmitter connected directly to the discriminator in a back-to-back configuration; the discriminator transmission function is also shown.

Prior to each set of measurements, the setting of the tunable bandpass filter used as the discriminator was optimized in the back-to-back configuration. The filter wavelength was adjusted while the photodetector signal was monitored on an RF spectrum analyzer, and the ratio of the fundamental to the second harmonic was maximized. Typically, this ratio was 22–23 dB, establishing a performance baseline for the link. As shown in Fig. 5(a), the optimum discriminator setting produced third and fourth harmonics well below $-50$ dB relative to the fundamental and higher harmonics below the noise floor of the measurement. Once optimized, the discriminator setting was held constant throughout the remainder of the experiment, and the second-harmonic ratio was verified again once the measurements were completed.

Harmonic-distortion data sets were collected in the back-to-back configuration, then with the 39.4-km length of standard fiber, then with the standard fiber compensated by DCF, and finally with the standard fiber compensated by the CFBG module. At each location, both the RF spectrum and the time-domain waveform of the demodulated photodetector signal were measured. These data sets are shown in Figs. 5 and 6, respectively. As expected, the harmonic distortion induced by the dispersion of the standard fiber is severe [Fig. 5(b)], producing a highly distorted time-domain signal [Fig. 6(b)].

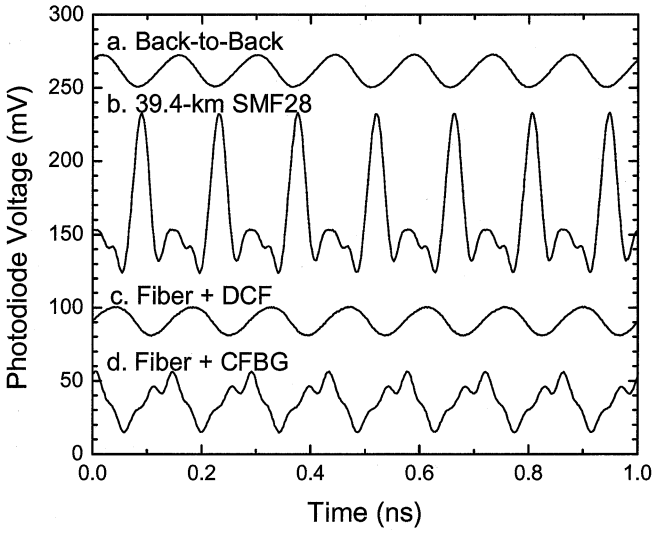


Fig. 6. 1550.000-nm demodulated time-domain waveforms at various points in the angle-modulated link: (a) back-to-back, (b) after 39.4 km of standard fiber, (c) the standard fiber compensated with DCF, and (d) the standard fiber compensated with the CFBG.

The DCF restores the signal nearly to the performance baseline of the back-to-back configuration [Figs. 5(c) and 6(c)], with only small increases in the relative powers of the higher harmonics indicating that the dispersion compensation is less than optimal. However, even though the DCF and the CFBG module display identical group-delay slopes, the link exhibits significant harmonic distortion when compensated by the CFBG module [Figs. 5(d) and 6(d)]. All measurable harmonics

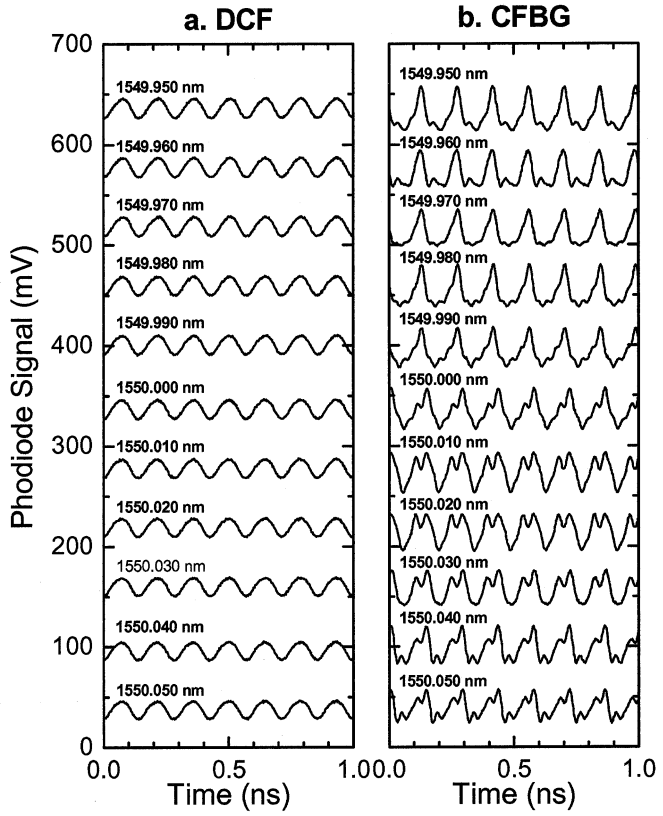


Fig. 7. Measured waveform distortion as a function of center wavelength when the link is compensated with (a) DCF and (b) the CFBG. The discriminator is held constant, optimized for 1550.000 nm.

display significant increases in relative power compared to the back-to-back case, and the time-domain waveform is clearly nonsinusoidal. This increased distortion is attributed to the ripple in the amplitude and delay response of the CFBG.

Two additional experimental results support this conclusion. First, the center wavelength was tuned by $\pm 50$ pm in 10-pm increments around 1550.000 nm with the modulation index held constant at $\beta = 1.9$ and the discriminator optimized for 1550.000 nm. Whereas the waveforms remain essentially sinusoidal when the link is compensated with DCF, the waveforms for the CFBG-compensated link evolve as the wavelength is tuned, with significant change in the waveform occurring on the order of every 30-40 pm (Fig. 7). This indicates that the relative contribution of the different sidebands is modified by the CFBG as the center wavelength is tuned, which is consistent with the presence of ripple in the CFBG transmission characteristics.

Second, the RF power delivered to the phase modulator was decreased in 3-dB increments, reducing the FM modulation index and therefore changing the relative contributions of the individual sidebands. As shown in the time-domain waveforms in Fig. 8, the demodulated signal again remains essentially sinusoidal when the link is compensated with DCF; however, the waveforms for the CFBG-compensated link vary with the applied RF signal power. The fact that the waveforms vary with RF power indicates that the sidebands experience different transmission coefficients, which again is consistent with the presence of ripple in the CFBG transmission characteristics.

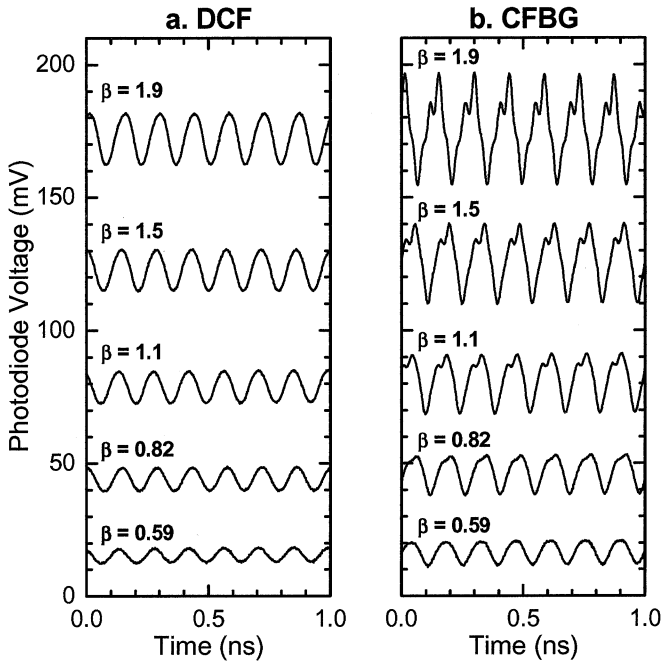


Fig. 8. Measured waveform distortion as a function of modulation index when the link is compensated with (a) DCF and (b) the CFBG. The center wavelength is 1550.000 nm and the modulation frequency is 7 GHz.

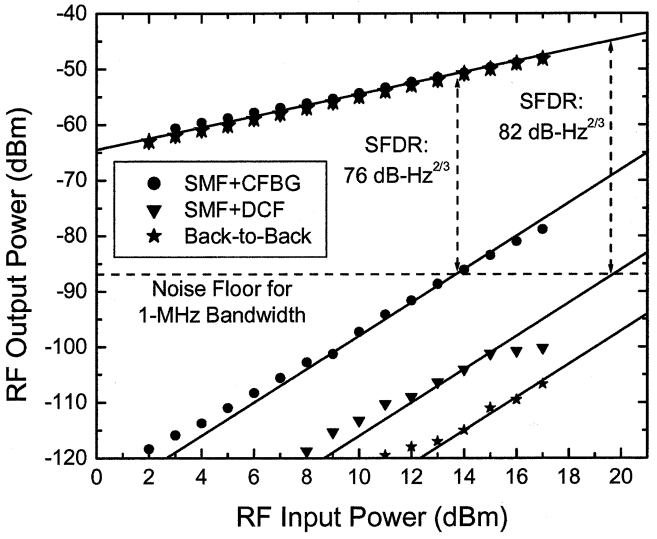


Fig. 9. Intermodulation distortion measured at 1550.000 nm with 7-GHz tones separated by 101 kHz.

### *D. Intermodulation Distortion Results*

While the harmonic distortion results presented above help elucidate the physical mechanism of the distortion, the effects of harmonic distortion can be minimized with proper filtering if the signal bandwidth is suboctave. In this case, third-order intermodulation products become the dominant distortion source, and thus two-tone measurements were performed to evaluate intermodulation distortion. The experimental configuration was identical to Fig. 1, with the exception that the phase modulator was driven by equal-amplitude tones at 7.0 and 7.000 101 GHz.

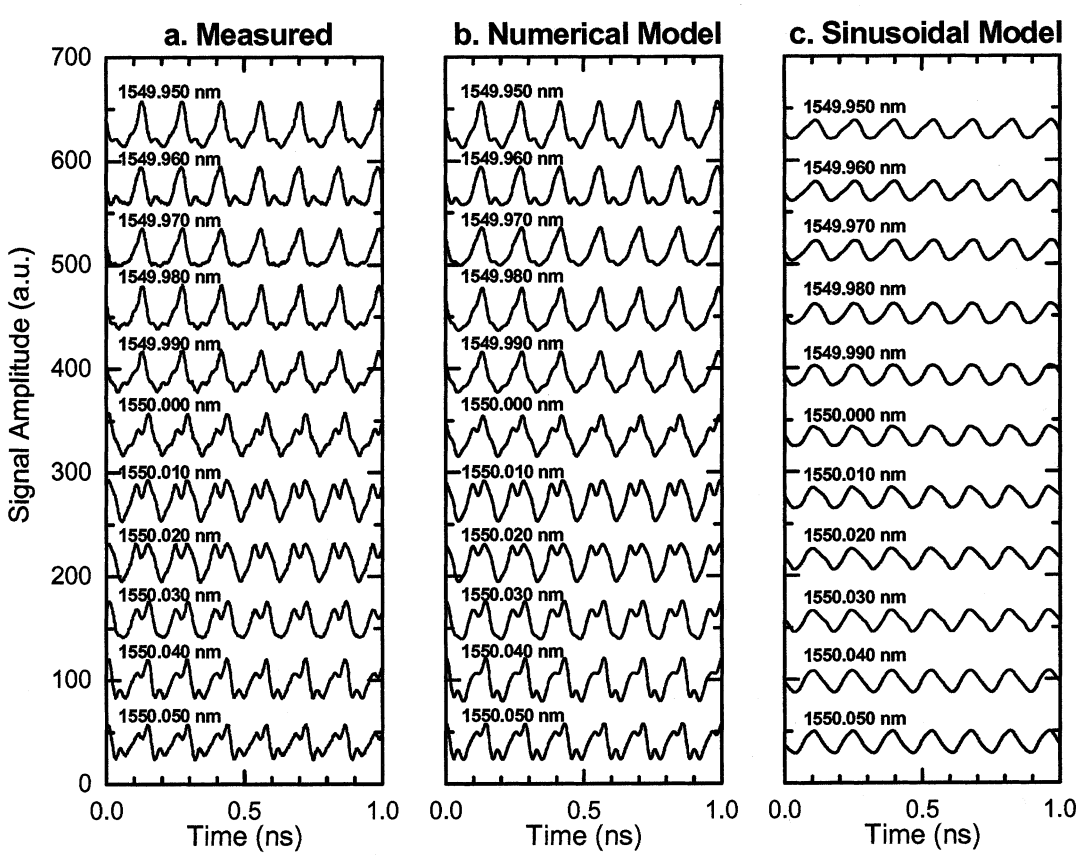


Fig. 10. Measured and simulated waveform distortion as a function of center wavelength when the link is compensated with the CFBG. The discriminator is held constant, optimized for 1550.000 nm.

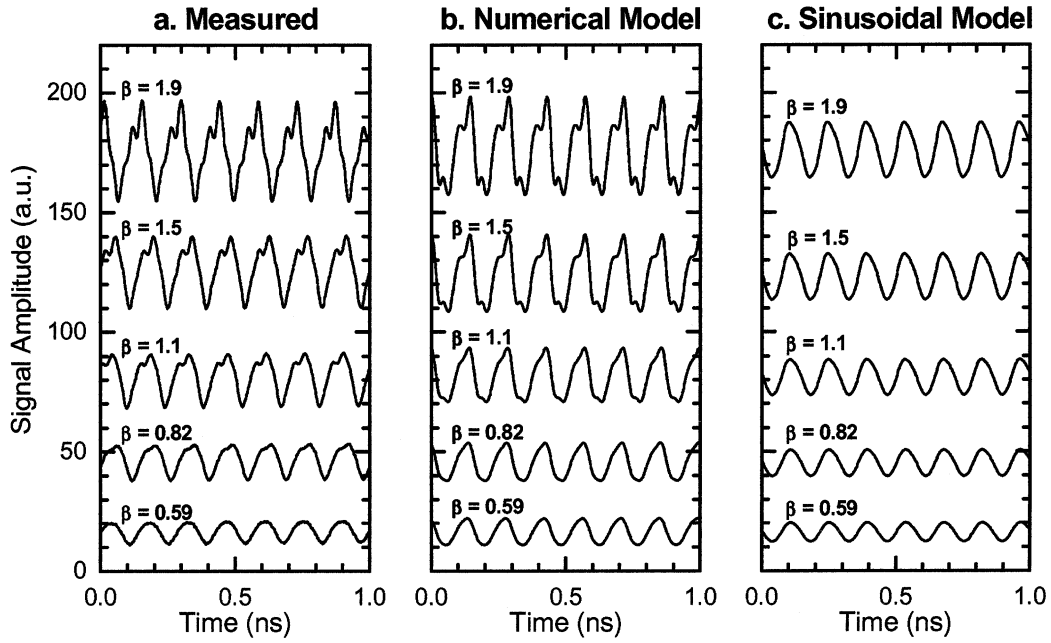


Fig. 11. Measured and simulated waveform distortion as a function of modulation index when the link is compensated with the CFBG. The center wavelength is 1550.000 nm and the modulation frequency is 7 GHz.

Fundamental and third-order intermodulation powers were measured with an RF spectrum analyzer as a function of RF power applied to the modulator. Data sets were collected for the back-to-back configuration, the standard fiber compensated by the DCF, and the standard fiber compensated by the CFBG module. As shown in Fig. 9, third-order intermodulation

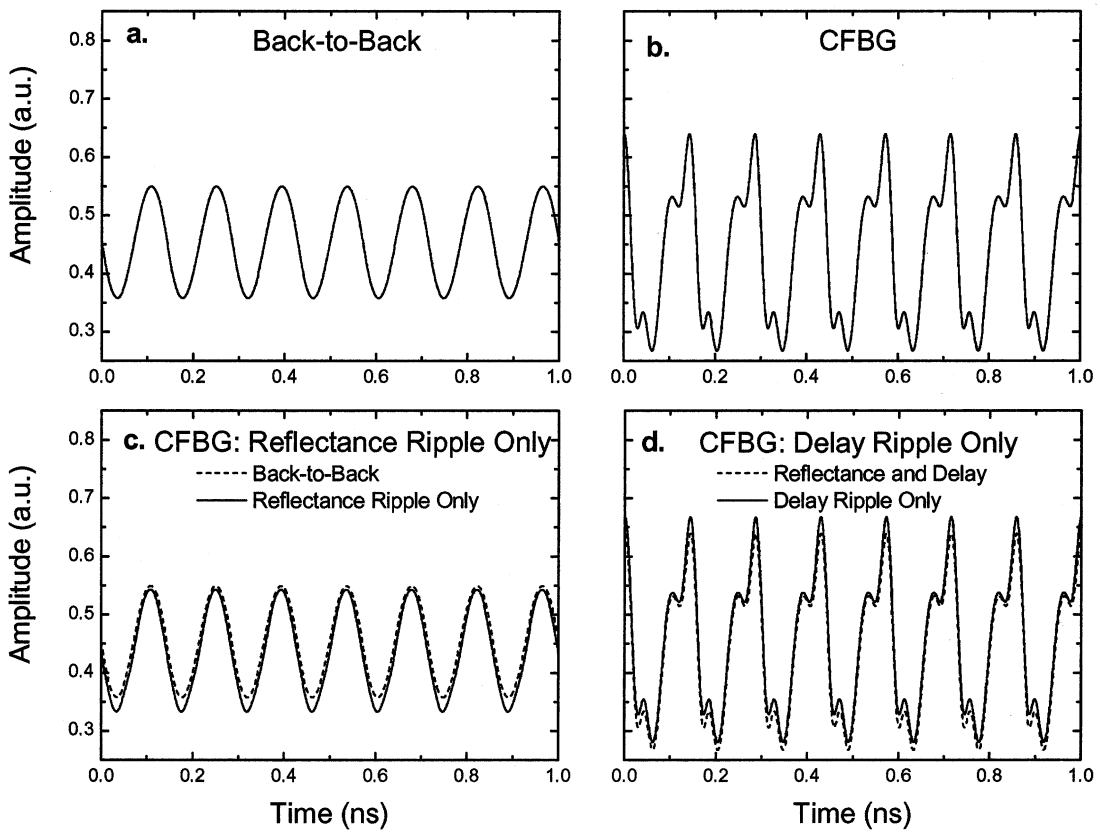


Fig. 12. Simulated waveforms for the link compensated by the CFBG. The modulation index is 1.9, the center wavelength is 1550.000 nm, and the modulation frequency is 7 GHz. The distortion is dominated by the delay ripple.

increases when the link is compensated with the CFBG instead of DCF, and there is a commensurate decrease in spur-free dynamic range from 82 to 76 dB-Hz$^{2/3}$.

## IV. Numerical Model

### A. Model Overview

The experimental results strongly indicate that the ripple in the CFBG amplitude and delay characteristics is responsible for the observed distortion. However, they do not indicate the relative contributions of these two mechanisms, and thus a numerical model was implemented to investigate the two independently. The input signal is modeled as an ideal FM signal with frequency-domain coefficients determined by (1). The link is treated as a linear filter with frequency response

$$H(\omega) = H_{\mathrm{CFBG}}(\omega) \cdot H_{\mathrm{BPF}}(\omega) \tag{7}$$

where

$$H_{\mathrm{CFBG}}(\omega) = \sqrt{T_{\mathrm{CFBG}}(\omega)} \exp\left(-i \int \tau_{\mathrm{CFBG}}(\omega)\, d\omega\right) \tag{8}$$

is the complex transfer function for the CFBG module, and likewise

$$H_{BPF}(\omega) = \sqrt{T_{\mathrm{BPF}}(\omega)} \exp\left(-i \int \tau_{\mathrm{BPF}}(\omega)\, d\omega\right) \tag{9}$$

is the complex transfer function for the bandpass filter used as a discriminator, which was determined in the same fashion as the CFBG transfer function. The average group delay of the compensated link is assumed to be constant, and therefore the phase of $H_{\mathrm{CFBG}}(\omega)$ represents the delay ripple of the CFBG module. Thus, the filter representing the channel and the FM discriminator is determined completely by experimentally determined parameters.

The demodulated time-domain signal at the receiver is constructed analytically using (1) with each frequency component appropriately weighted in amplitude and phase via (7). Eight pairs of sidebands are retained for the calculations, which is more than sufficient for the modulation indexes considered here ($\beta < 2$). The demodulated signal is square-law detected and the envelope is recovered with a numerical envelope detector based on peak detection and interpolation. For completeness, the resulting intensity-modulated signal is then filtered using the experimentally determined response of the photodetector and oscilloscope, although this was found to have a negligible impact on the results. To produce a reference signal for comparison, the back-to-back signal is calculated with $H_{\mathrm{CFBG}}(\omega)$ set equal to unity, thus incorporating the nonideal performance of the discriminator without including the ripple from the CFBG. To quantify this comparison, the mean square error between the back-to-back and distorted signal envelopes is calculated using

$$\varepsilon = \frac{1}{T} \int_0^T \left[e_{\mathrm{distorted}}(t) - e_{\mathrm{back-to-back}}(t)\right]^2 dt. \tag{10}$$

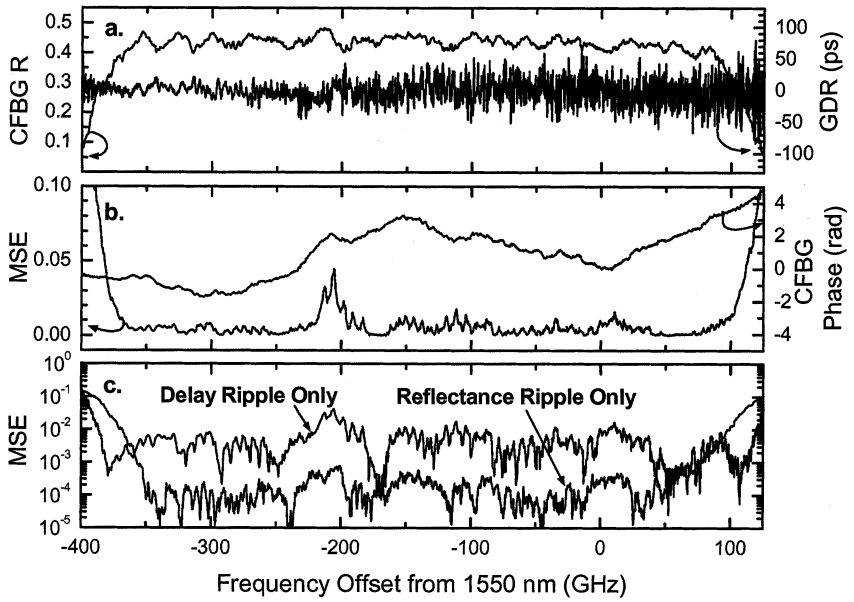


Fig. 13. Calculated mean square error as a function of wavelength for the link compensated by the CFBG. The modulation index is 1.9 and the modulation frequency is 7 GHz. (a) CFBG reflectance and group-delay ripple. (b) Total mean square error and CFBG phase determined from the measured group delay. (c) Components of the mean square error due to the delay ripple and the reflectance ripple.

### *B. Numerical Results*

The model was verified by reproducing the experimental harmonic distortion presented above in Figs. 7 and 8. First, the FM modulation index was held constant at $\beta = 1.9$ while the laser wavelength was tuned. As in the experiment, the bandpass filter used as a discriminator was held constant, optimized for 1550.000 nm. The only adjustable parameter in the simulation was the absolute wavelength of the CFBG characteristics, which was observed to vary slightly as a function of measurement instrument and input polarization during initial characterization. The data sets presented in Fig. 10 were obtained with a shift of 18 pm from the nominal wavelength determined during initial characterization; the agreement between the simulated and measured data is excellent. As discussed below, the waveforms were also generated using the sinusoidal model for delay ripple (5) with $A_{\mathrm{GDR}} = 40$ ps and $T_{\mathrm{GDR}} = 650$ MHz [Fig. 10(c)]. In Fig. 11, the FM modulation index in the model was varied using the values determined from the measured optical spectra to model the harmonic distortion as a function of applied RF power. The results are again in good agreement with the measured data, and the results using the sinusoidal model for delay ripple are again shown for comparison [Fig. 11(c)]. All of the main features in both sets of measured waveforms are reproduced by the simulation, thereby validating the numerical model.

Next, the relative contributions of the reflectance and delay ripple were determined by evaluating each independently. In Fig. 12(a) and (b), the simulated back-to-back and CFBG-compensated cases corresponding to the measured data in Fig. 6(a) and (d) are shown. In Fig. 12(c), the simulation was performed with the delay ripple set to zero so that only the reflectance ripple is included; likewise, in Fig. 12(d), only the delay ripple was included. The results clearly show that the distortion for this particular CFBG is dominated by the delay ripple; however, the reflectance ripple also makes a small contribution. Obviously, the relative contributions of the two distortion mechanisms will vary among different CFBGs with the relative amplitudes and periods of the reflectance and delay ripple.

Likewise, the relative contributions will vary as a function of wavelength within a given CFBG because the reflectance and delay ripples are dissimilar. To quantify this effect, the mean square error was calculated as a function of wavelength by tuning the laser and discriminator relative to the CFBG. The modulation frequency was again set to 7 GHz and the FM modulation index was set to $\beta = 1.9$. The calculation was first performed with both the reflectance and delay ripple included; the results are shown in Fig. 13 along with the measured CFBG reflectance and group-delay characteristics. The mean square error is relatively constant across most of the bandwidth of the CFBG, with some significant peaks in the region around 1551.644 nm (-205 GHz). Note the rapid increase in error at the edges of the grating where some of the sidebands are no longer within the CFBG reflection band. The calculation was then repeated with the reflectance and delay ripple selectively turned off; the results are shown in Fig. 13(c), and again indicate that the delay ripple is the dominant distortion mechanism for this particular grating.

Returning now to Figs. 10 and 11, the sinusoidal model for delay ripple clearly does not reproduce the observed waveforms. The reason can be understood from Fig. 14, where the ripple-induced component of the phase is shown along with the CFBG reflectance and delay ripple in the region around 1550 nm. The phase determined from the measured group delay using (3) displays significantly larger deviations than that determined using the sinusoidal model via (6). As is evident in both Figs. 3 and 14, the local period of the delay ripple for this grating is not well defined, and large deviations in phase can occur. Thus,

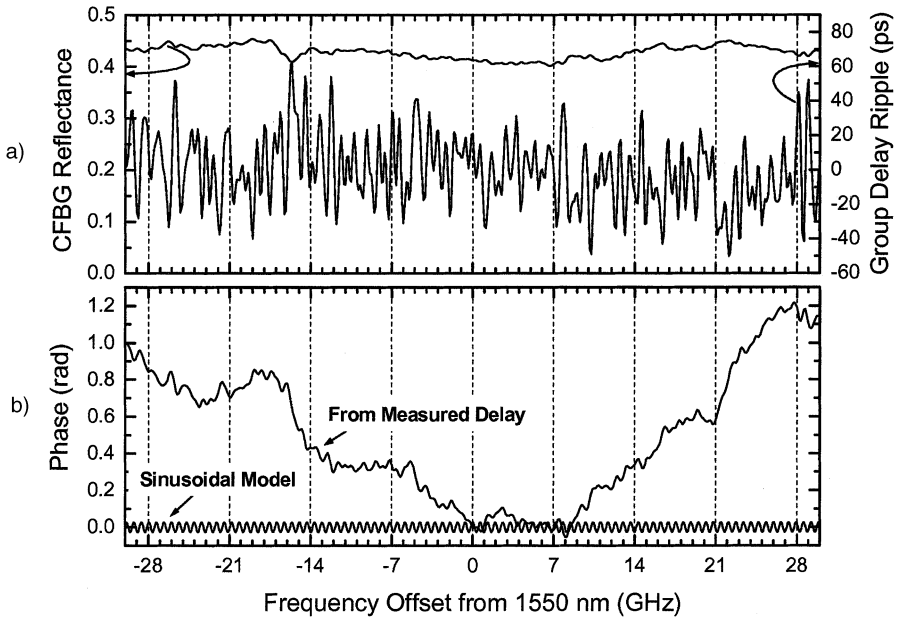


Fig. 14. (a) Transmission and group-delay ripple of the CFBG module in the region near 1550.000 nm. (b) The phase associated with the CFBG delay ripple determined from the measured group delay and the sinusoidal model.

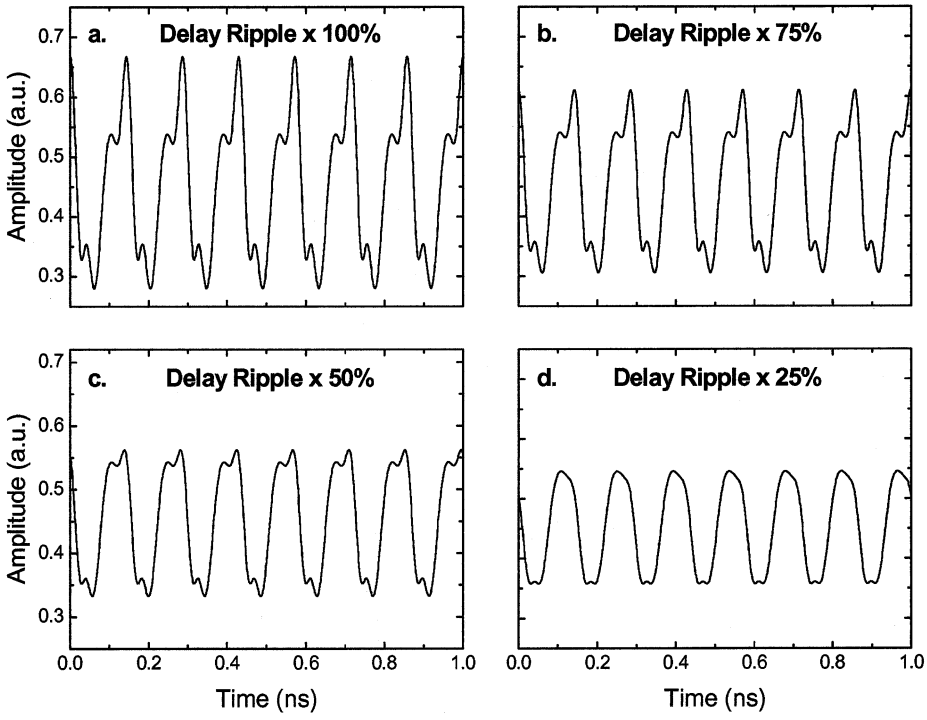


Fig. 15. Simulated waveforms as a function of delay-ripple amplitude for the link compensated by the CFBG. The modulation index is 1.9, the center wavelength is 1550.000 nm, and the modulation frequency is 7 GHz.

random imperfections in fabrication can greatly exacerbate the phase distortion. With optimized fabrication, the phase distortion could potentially be reduced to the level implied by the product $A_{\mathrm{GDR}} \cdot T_{\mathrm{GDR}}$ in the sinusoidal model, which is on the order of tens of milliradians for this grating and could be even smaller with optimized apodization.

In Fig. 15, the distorted waveform is shown as a function of delay-ripple amplitude. In these calculations, the reflectance ripple was again set to zero and the delay ripple was multiplied by (a) 100%, (b) 75%, (c) 50%, and (d) 25%. The other simulation parameters were $\lambda = 1550.000$ nm, $\Omega_m/2\pi = 7$ GHz, and $\beta = 1.9$. The mean square error was found to increase with the amplitude of the delay ripple.

Finally, the mean square error was calculated as a function of modulation frequency. Both the reflectance and delay ripple were included, and once again $\beta = 1.9$. Calculations were per-

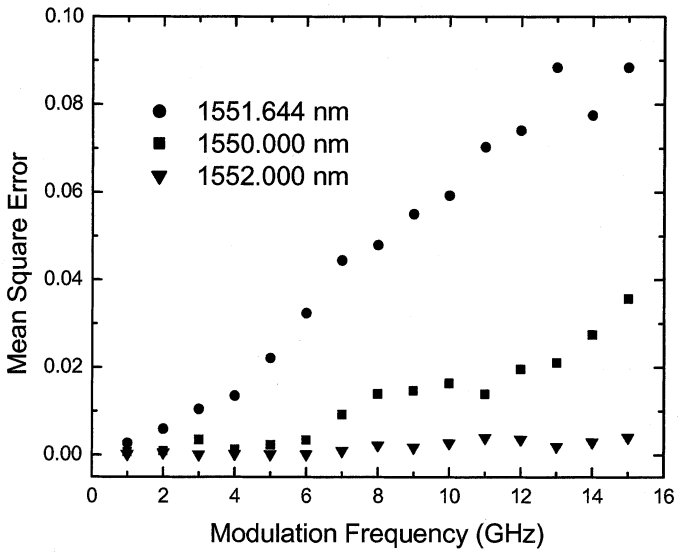


Fig. 16. Calculated mean square error as a function of modulation frequency. The modulation index is 1.9.

formed for three different wavelengths: 1550.000, 1552.000, and 1551.644 nm, where the error predicted in Fig. 13 is at a maximum. The results are shown in Fig. 16 and confirm that the error is larger at 1551.644 nm. Interestingly, the error increases with modulation frequency; note that the period of the delay ripple is $< 1$ GHz, and thus the frequency span between adjacent sidebands of the angle-modulated signal corresponds to multiple periods of delay ripple for all modulation frequencies considered.

## V. Conclusion

The ripple in both the delay and the amplitude response of chirped fiber Bragg gratings has been shown to produce distortion in wide-band angle-modulated fiber-optic links. Wide-band angle modulation is especially susceptible to these ripple effects because the signal information is spread over multiple sidebands, each of which experiences a different shift in both amplitude and phase upon reflection from the CFBG. Experimental results with a commercial CFBG dispersion compensation module reveal significant harmonic and intermodulation distortion, even when the average group delay of the link is very nearly constant with wavelength. Numerical modeling has shown that the residual delay ripple is the dominant source of distortion with the particular CFBG used in these experiments, and that the phase distortion associated with random fabrication errors can be especially large. Absolute performance levels for a given grating are a function of wavelength, modulation frequency, and modulation index. For dispersion-compensation applications, the ripple-induced distortion may tend to encourage the use of DCF rather than CFBGs. The ramifications are more problematic for advanced signal-processing applications that are based on CFBGs, and careful minimization of amplitude and delay ripple may be necessary to achieve the desired performance.

## Acknowledgment

The author is grateful to J. C. Gottschalk, P. W. Juodawlkis, S. A. Hamilton, B. S. Robinson, and B. R. Washburn for useful discussions and the loan of equipment, and to P. A. Schulz, R. R. Patel, and S. J. Savage for facilitating group-delay measurements.

## References

[1] R. Kashyap, *Fiber Bragg Gratings*. San Diego, CA: Academic, 1999.
[2] A. Othonos and K. Kalli, *Fiber Bragg Gratings.* Boston, MA: Artech House, 1999.
[3] D. R. Giles, "Ligtwave applications of fiber Bragg gratings," *J. Lightwave Technol.*, vol. 15, pp. 1391–1404, Aug. 1997.
[4] I. Bennion, J. A. R. Williams, L. Zhang, K. Sugden, and N. J. Doran, "UV-written in-fiber Bragg gratings," *Opt. Quantum Electron.*, vol. 28, pp. 93–115, 1996.
[5] T. Erdogan, "Fiber grating spectra," *J. Lightwave Technol.*, vol. 15, pp. 1277–1294, Aug. 1997.
[6] B. J. Eggleton, A. Ahuja, P. S. Westbrook, J. A. Rogers, P. Kuo, T. N. Nielsen, and B. Mikkelsen, "Integrated tunable fiber gratings for dispersion management in high-bit rate systems," *J. Lightwave Technol.*, vol. 18, pp. 1418–1432, Oct. 2000.
[7] M. Sumetsky, B. J. Eggleton, and C. M. Sterke, "Theory of group delay ripple generated by chirped fiber gratings," *Opt. Express*, vol. 10, pp. 332–340, Apr. 2002.
[8] T. Komukai, T. Inui, and M. Nakazawa, "The design of dispersion equalizers using chirped fiber Bragg gratings," *IEEE J. Quantum Electron.*, vol. 36, pp. 409–417, Apr. 2000.
[9] T. Inui, T. Komukai, M. Nakazawa, K. Suzuki, K. R. Tamura, K. Uchiyama, and T. Morioka, "Adaptive dispersion slope equalizer using a nonlinearly chirped fiber Bragg grating pair with a novel dispersion detection technique," *IEEE Photon. Technol. Lett.*, vol. 14, pp. 549–551, Apr. 2002.
[10] J. Brennan, "Dispersion management with long-length fiber Bragg gratings," presented at the Optical Fiber Communication Conf., Atlanta, GA, Mar. 23–28, 2003, paper FC1.
[11] F. Devaux, Y. Sorel, and J. F. Kerdiles, "Simple measurement of fiber dispersion and of chirp parameter of intensity modulated light emitter," *J. Lightwave Technol.*, vol. 11, pp. 1937–1940, Dec. 1993.
[12] H. Schmuck, "Comparison of optical millimeter-wave system concepts with regard to chromatic dispersion," *Electron. Lett.*, vol. 31, pp. 1848–1849, Oct. 1995.
[13] W. I. Way, *Broadband Hybrid Fiber/Coax Access System Technologies*. San Diego, CA: Academic, 1999, pp. 358–361.
[14] P. C. Chou, H. A. Haus, and J. F. Brennan III, "Reconfigurable time-domain spectral shaping of an optical pulse stretched by a fiber Bragg grating," *Opt. Lett.*, vol. 25, pp. 524–526, Apr. 2000.
[15] S. Lee, R. Khosravani, J. Peng, V. Grubsky, D. S. Starodubov, A. E. Willner, and J. Feinberg, "Adjustable compensation of polarization mode dispersion using a high-birefringence nonlinearly chirped fiber Bragg grating," *IEEE Photon. Technol. Lett.*, vol. 11, pp. 1277–1279, Oct. 1999.
[16] J. C. Chen and R. A. Brown, "Novel optical frequency discriminator with "perfect" linearity," presented at the Optical Fiber Communication Conf., Baltimore, MD, Mar. 7–10, 2000, Paper WM40.
[17] X. Xie, J. B. Khurgin, J. U. Kang, and F. S. Choa, "Compact linearized optical FM discriminator," *IEEE Photon. Technol. Lett.*, vol. 14, pp. 384–386, Mar. 2002.
[18] R. Kashyap, *Fiber Bragg Gratings*. San Diego, CA: Academic, 1999, pp. 311–353.
[19] K. Ennser, M. Ibsen, M. Durkin, M. N. Zervas, and R. I. Laming, "Influence of nonideal chirped fiber grating characteristics on dispersion cancellation," *IEEE Photon. Technol. Lett.*, vol. 10, pp. 1476–1478, Oct. 1998.
[20] S. G. Evangelides Jr, N. S. Bergano, and C. R. Davidson, "Intersymbol interference induced by delay ripple in fiber Bragg gratings," presented at the Optical Fiber Communication Conf., San Diego, CA, Feb. 21–26, 1999, Paper FA2.
[21] A. Sahara, T. Komukai, E. Yamada, and M. Nakazawa, "40 Gbit/s return-to-zero transmission over 500 km of standard fiber using chirped fiber Bragg gratings with small group delay ripples," *Electron. Lett.*, vol. 37, pp. 8–9, Jan. 2001.

[22] S. Jamal and J. C. Cartledge, "Variation in the performance of multispan 10-Gb/s systems due to the group delay ripple of dispersion compensating fiber Bragg gratings," *J. Lightwave Technol.*, vol. 20, pp. 28–35, Jan. 2002.
[23] L. Zhu, M. Chen, Y. Zhang, and S. Xie, "Impacts of cascaded filters with group delay ripples on 40-Gb/s WDM transmission system," *IEEE Photon. Technol. Lett.*, vol. 14, pp. 1518–1520, Nov. 2002.
[24] N. Litchinitser, Y. Li, M. Sumetsky, P. Westbrook, and B. Eggleton, "Tunable dispersion compensation devices: Group delay ripple and system performance," presented at the Optical Fiber Communication Conf., Atlanta, GA, Mar. 23–28, 2003, paper TuD2.
[25] X. Fan, D. Labrake, and J. Brennan, "Chirped fiber grating characterization with phase ripples," presented at the Optical Fiber Communication Conf., Atlanta, GA, Mar. 23–28, 2003, paper FC2.
[26] D. Pastor, J. Capmany, and J. Martí, "Reduction of dispersion induced composite triple beat and second-order intermodulation in subcarrier multiplexed systems using fiber grating equalizers," *IEEE Photon. Technol. Lett.*, vol. 9, pp. 1280–1282, Sept. 1997.
[27] J. Martí, J. M. Fuster, and R. I. Laming, "Experimental reduction of chromatic dispersion effects in lightwave microwave/millimeter-wave transmission using tapered linearly chirped fiber gratings," *Electron. Lett.*, vol. 33, pp. 1170–1171, June 1997.
[28] F. Ramos and J. Marti, "Influence of nonideal chirped fiber grating characteristics on dispersion-compensated analogue optical links in presence of fiber-induced SPM," *Electron. Lett.*, vol. 39, pp. 353–355, Feb. 2003.
[29] D. Garthe, G. Milner, and Y. Cai, "System performance of broadband dispersion compensating gratings," *Electron. Lett.*, vol. 34, pp. 582–583, Mar. 1998.
[30] L. R. Chen, "Influence of grating group delay ripple on the reduction of dispersion induced intensity noise in subcarrier multiplexed systems," *Opt. Commun.*, vol. 187, pp. 125–128, Jan. 2001.
[31] P. Broson, C. A. Ribeiro, and J. E. Ripper, "Frequency demodulation of a semiconductor laser by FM-AM conversion in an optical fiber," *IEEE J. Quantum Electron.*, vol. QE-17, pp. 689–693, May 1981.
[32] A. R. Chraplyvy, R. W. Tkach, L. L. Buhl, and R. C. Alferness, "Phase modulation to amplitude modulation conversion of CW laser light in optical fibers," *Electron. Lett.*, vol. 22, pp. 409–411, April 1986.
[33] B. P. Lathi, *Modern Digital and Analog Communication Systems*, 2nd ed. Philadelphia, PA: Holt, Rinehart and Winston, 1989, pp. 294–340.
[34] R. Kashyap, *Fiber Bragg Gratings*. San Diego, CA: Academic Press, 1999, pp. 409–446.
[35] P. Hernday, "Dispersion measurements," in *Fiber Optic Test and Measurement*, D. Derrickson, Ed. Upper Saddle River, NJ: Prentice-Hall, 1998, pp. 475–518.
[36] T. Niemi, M. Uusimaa, and H. Ludvigsen, "Limitations of phase-shift method in measuring dense group delay ripple of fiber Bragg gratings," *IEEE Photon. Technol. Lett.*, vol. 13, pp. 1334–1336, Dec. 2001.
[37] G. Genty, T. Niemi, and H. Ludvigsen, "New method to improve the accuracy of group delay measurements using the phase-shift technique," *Opt. Commun.*, vol. 204, pp. 119–126, April 2002.
[38] G. D. VanWiggeren, A. R. Motamedi, B. Szafraniec, R. S. Tucker, and D. M. Baney, "Single-scan polarization-resolved heterodyne optical network analyzer," presented at the Optical Fiber Communication Conf., Anaheim, CA, Mar. 17–22, 2002, paper WK2.

**Todd G. Ulmer** (M'93) was born in Pennsylvania in 1970. He received the B.S. degree in physics *(magna cum laude)* from Furman University, Greenville, SC, in 1993, the B.E.E. degree (with highest honors) from the Georgia Institute of Technology (Georgia Tech), Atlanta, in 1994, and the M.S. and Ph. D. degrees in electrical engineering from Georgia Tech in 1996 and 2000, respectively.

From 1993 to 2000, he was a Member of the Ultrafast Optical Communications group in Georgia Tech's Microelectronics Research Center. His dissertation research involved an integrated-optical serial-to-parallel converter for optical time-division demultiplexing that utilized microcavity-enhanced surface-emitted second-harmonic generation in semiconductor waveguides. In 2001, he joined the Optical Communications Technology group, Lincoln Laboratory, Massachusetts Institute of Technology, where he is presently investigating free-space optical communications, wideband analog optical links, fiber Bragg gratings, and automatic polarization control. His research interests also include optical time-division multiplexing, nonlinear optics in semiconductors and optical fiber, integrated optical devices, and optical switching.

Dr. Ulmer is a Member of Phi Beta Kappa, Eta Kappa Nu, Tau Beta Pi, the IEEE Lasers and Electro-Optics Society (LEOS), and the Optical Society of America (OSA). He received a Schlumberger Foundation Fellowship and a 2000 SAIC student paper award.